(a)

(b)

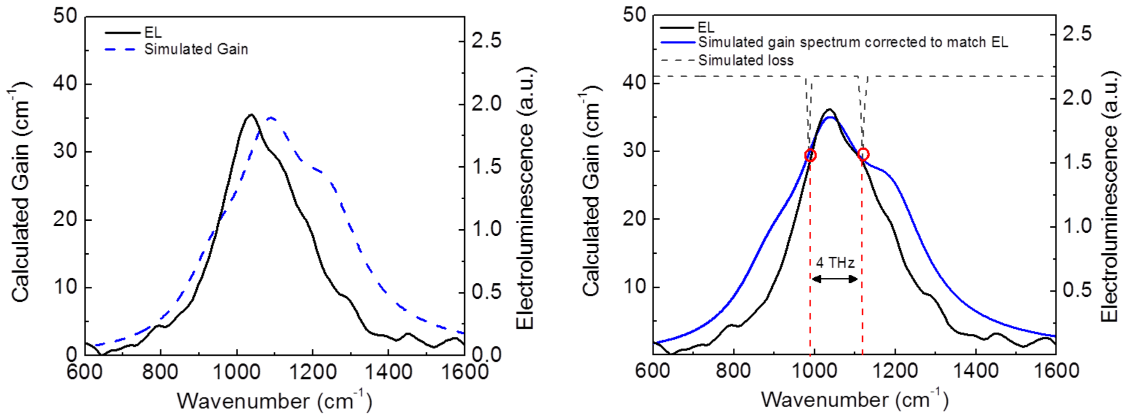

Supplementary Figure S1, Simulated and measured mid-IR gain spectrum of the active regions: (a) Simulated gain spectrum (blue line, bottom and right axis) and electroluminescence (black line, bottom and left axis). Electroluminescence (EL) measurements were done at 298 K with a 200 µm-diameter mesa cleaved in half and operated at a current density of 7 kA/cm^2. (b) Simulated gain red-shifted 50 cm^{-1} to match EL spectrum. DFBs were used to select mid-IR lasing at 1120 cm^{-1} and 986 cm^{-1} (shown in red), corresponding to 4 THz. The population density in the upper laser state clamps when the gain at these two lasing frequencies equals the loss (shown in grey).

Supplementary Note 1: Calculation of χ⁽²⁾ in the QCL active region

Our method for calculating $\chi^{(2)}$ for the active regions presented in Fig. 2 follows a similar approach described in Ref. 11. We use the fully-resonant quantum-mechanical expression for $\chi^{(2)}$ given as[19]:

$$\chi^{(2)}(\omega_{DFG}=\omega_p-\omega_q,\omega_p,-\omega_q)=\Delta N\frac{e^3}{\varepsilon_o\hbar^2}\sum_{lmn}\rho_{ll}^{(0)}\left\{\begin{aligned}&\frac{z_{ln}z_{nm}z_{ml}}{\left[\left(\omega_{nl}-\omega_{DFG}\right)-i\Gamma_{nl}\right]\left[\left(\omega_{ml}-\omega_p\right)-i\Gamma_{ml}\right]}\\&+\frac{z_{ln}z_{nm}z_{ml}}{\left[\left(\omega_{nl}-\omega_{DFG}\right)-i\Gamma_{nl}\right]\left[\left(\omega_{ml}+\omega_q\right)-i\Gamma_{ml}\right]}\\&+\frac{z_{ln}z_{nm}z_{ml}}{\left[\left(\omega_{mn}-\omega_{DFG}\right)-i\Gamma_{nl}\right]\left[\left(\omega_{nl}+\omega_p\right)+i\Gamma_{nl}\right]}\\&+\frac{z_{ln}z_{nm}z_{ml}}{\left[\left(\omega_{mn}-\omega_{DFG}\right)-i\Gamma_{nl}\right]\left[\left(\omega_{nl}-\omega_q\right)+i\Gamma_{nl}\right]}\\&+\frac{z_{ln}z_{nm}z_{ml}}{\left[\left(\omega_{nm}+\omega_{DFG}\right)+i\Gamma_{nl}\right]\left[\left(\omega_{ml}-\omega_p\right)-i\Gamma_{ml}\right]}\\&+\frac{z_{ln}z_{nm}z_{ml}}{\left[\left(\omega_{nm}+\omega_{DFG}\right)+i\Gamma_{nl}\right]\left[\left(\omega_{ml}+\omega_q\right)-i\Gamma_{ml}\right]}\\&+\frac{z_{ln}z_{nm}z_{ml}}{\left[\left(\omega_{ml}+\omega_{DFG}\right)+i\Gamma_{nl}\right]\left[\left(\omega_{nl}+\omega_p\right)+i\Gamma_{nl}\right]}\\&+\frac{z_{ln}z_{nm}z_{ml}}{\left[\left(\omega_{ml}+\omega_{DFG}\right)+i\Gamma_{nl}\right]\left[\left(\omega_{nl}-\omega_q\right)+i\Gamma_{nl}\right]}\end{aligned}\right\} \tag{S1}$$

where the indices l,m,n correspond to the energy levels that take part in DFG, ΔN is the population inversion density and ez_{ij}, ω_{ij} and Γ_{ij} are the dipole matrix element, frequency, and broadening of the transition between states *i* and *j*. Applying this equation to our structures (see Fig. 2(a,b)), we set l=1, and permute m and n over all combinations of the lower state energy levels. This results in 16 terms and 32 terms for the active regions presented in Fig. 2(a,b), respectively, and is too long to write here. Values for energy levels and dipole matrix elements were found using a self-consistent Schrödinger-Poisson solver and given in the Fig. 2 caption. Values for the transition linewidth between states were chosen by comparing data from different literature sources[30,31,32]; here we used a full-width of half-max of Γ = 12.5 meV and Γ = 4 meV for the mid-infrared and THz transitions, respectively.

To evaluate $\chi^{(2)}$, we need to calculate the population difference ΔN between DFG states. In our structures, state 1 coincides with the upper laser level and all other DFG states coincide with the lower laser levels (see Fig. 2(a,b)). We can therefore approximate ΔN as being equal to the upper state population and assume the same population density in each active region. This can be found by applying the "gain = loss" condition for a laser given as:

$$\frac{g_{1,\omega}+g_{2,\omega}}{2}=\frac{\alpha_m+\alpha_w}{\Gamma} \qquad \text{(S2)}$$

where Γ, $g_{i\omega}$, α_w, α_m, and g_{max} is the mid-infrared modal overlap with the active region core (with includes both active region stacks) at frequency *ω*, the gain in active region *i* at frequency *ω*, waveguide loss, mirror loss, and maximum gain at which clamping occurs, respectively. We simulate our structure using COMSOL and find that Γ = 0.84, $\alpha_w \approx 8$ cm^{-1} and $\alpha_m \approx 6$ cm^{-1} for a 2mm-long device with uncoated facets. This results in $g_{max} \approx 30$ cm^{-1}.

Next, we calculate the gain spectrum for each active region stack using the QCL gain expression given as:

$$g(\omega_i)=\frac{\omega_i}{cn_{eff}(\omega_i)}\frac{\Delta N}{\varepsilon_0\hbar}\mathrm{Im}\left(\sum_n\frac{\left|e\cdot z_{1n}\right|^2}{(\omega_i-\omega_{1n})-i\cdot\Gamma_{1n}}\right) \qquad \text{(S3)}$$

where n_{eff} is the effective modal index at frequency ω_i. The simulated gain spectrum for both active regions combined and the measured electroluminescence (EL) is presented in Supplementary Fig. S1(a). The EL spectrum is red-shifted by 50 cm^{-1} compared to the simulation. We attribute this shift to uncertainty in the growth parameters (i.e. layer thicknesses, doping, etc.). We can reconcile the differences in the measured/simulated spectrum by shifting the simulated gain spectrum to overlay with the EL spectrum as shown in Supplementary Fig. S1(b). We note that we still assume the same values for the transition dipole moments simulated in the 'pre-shifted' structure.

For our 4 THz source, DFBs were used to select the mid-IR pumps at λ_1 = 1120cm^{-1} and λ_2 = 986cm^{-1}, see Fig.4a. The mid-IR loss in DFB devices remains virtually unchanged, compared to Fabry-Perot lasers, at these two wavelengths[23,33]. We can verify this fact by noting that the threshold current density remains around the same for Fabry-Perot and grating-based devices. As a result, the population will clamp when the gain at either lasing wavelengths reaches the loss.

Given that the gain cross-section at both lasing wavelengths is nearly the same, we calculate ΔN ≈ 8.5x10^{14} cm^{-3}. Using this value we calculate $\chi^{(2)}$ = 21,000 - i*7,500 pm/V and $\chi^{(2)}$ = 9,000 - i*4,000 pm/V for the active regions presented in Fig. 2a and Fig. 2b, respectively.

We note that we used slightly larger linewidths for the mid-IR transitions, compared to that used in Refs. 11 and 12, and fixed computing errors made in these references, which resulted in reduction of theoretical values of $\chi^{(2)}$ in all structures. The new linewidth values are more consistent with experimental measurements[30,31,32].

Supplementary References

30. Capasso F., Sirtori C., and Cho A.Y. Coupled quantum well semiconductors with giant electric field tunable nonlinear optical properties in the infrared. *IEEE Journal of Quantum Electronics*, **30** 1313 (1994).
31. Dupont E., Wasilewski Z. R., and Liu H. C. Terahertz emission in asymmetric quantum wells by frequency mixing of midinfrared waves. *Journal of Quantum Electronics*, **42**, 1157 (2006).
32. Scheinert M., Sigg H., Tsujino S., Giovannini M., and Faist, J. Intersubband Raman laser from GaInAs/AlInAs double quantum wells. *Applied Physics Letters*, **91**, 131108 (2007).
33. Carras M. and De Rossi A. Photonic modes of metallodielectric periodic waveguides in the midinfrared spectral range. *Phys. Rev. B* **74,** 235120 (2006).